# Rearrangement of the orbital-ordered state at the metal-insulator transition of $La_{7/8}Sr_{1/8}MnO_3$

J. Geck,[1,2] P. Wochner,[2] D. Bruns,[1] B. Büchner,[1] U. Gebhardt,[2] S. Kiele,[1,3] P. Reutler,[1,4] and A. Revcolevschi[4]
[1]*Physikalisches Institut, RWTH Aachen, 52056 Aachen, Germany*
[2]*Max-Planck-Institut für Metallforschung, Heisenberg Str. 3, 70569 Stuttgart, Germany*
[3]*Hamburger Synchrotronstrahlungslabor HASYLAB at Deutsches Elektronen-Synchrotron DESY, Notkestr. 85, 22603 Hamburg, Germany*
[4]*Laboratoire de Physico-Chimie de l'Etat Solide, Université de Paris-Sud, 91405 Orsay Cedex, France*
(Received 6 June 2003; revised manuscript received 3 December 2003; published 19 March 2004)

We present a resonant x-ray scattering study at the manganese *K* edge on $La_{7/8}Sr_{1/8}MnO_3$ at temperatures between 10 K and 310 K along with thermal expansion, magnetization, and electrical resistivity measurements. At the Mn *K* edge the symmetry-forbidden (300) reflection is observed in the whole temperature range under investigation and its integrated intensity is found to be directly connected to structural distortions. In particular, the intensity of the (300) reflection increases strongly in the cooperative Jahn-Teller distorted phase between 150 K and 270 K. The increase of the resonant intensity in this temperature regime, the rotation of the beam polarization from $\sigma$ to $\pi$, the $\sin^2$-azimuthal dependence and the anomalies displayed by the lattice constants give firm experimental evidence for an orbital ordered state between 150 K and 270 K similar to that found in $LaMnO_3$. Upon cooling, the intensity of the (300) reflection collapses at the charge ordering temperature $T_{CO}=150$ K and the resonant (1.5,1.5,3) superstructure reflection emerges. This reflection also displays a resonant behavior at the Mn *K* edge and a pronounced azimuthal dependence. However, a resonant signal is observed in the $\sigma\sigma$ as well as in the $\sigma\pi$ channel. The results reveal that the metal-insulator transition of $La_{7/8}Sr_{1/8}MnO_3$ is accompanied by an orbital reordering.

DOI: 10.1103/PhysRevB.69.104413 PACS number(s): 71.30.+h, 61.10.Eq, 64.60.Cn, 71.27.+a

## I. INTRODUCTION

One focus of current condensed matter research is the investigation of strong electronic correlations in transition metal oxides. The interactions between structure, magnetism, and charges result in a variety of intriguing phenomena like high-temperature superconductivity,[1] charge ordering phenomena[2–5] and the colossal magnetoresistance effect in the doped manganites.[6,7] In the case of manganites, however, not only the charge and spin of the charge carriers have to be taken into account. It is the orbital degree of freedom which has recently turned out to be one of the key parameters for the understanding of the physical properties of doped manganites.[7]

A prominent and well-established example for the role of the orbital degree of freedom is the cooperative Jahn-Teller distorted phase of $LaMnO_3$ which is observed below $T_{JT} \simeq 780$ K.[8–10] In this compound only Jahn-Teller-active $Mn^{3+}$-ions are present and below $T_{JT}$ an antiferro-orbital ordering occurs within the $ab$ plane, as illustrated in Fig. 1. In this phase the elongated axis of one Jahn-Teller distorted octahedra points to the short axes of its neighbors, resulting in a gain of elastic energy. However, it is not only the antiferrodistortive ordering of the octahedra which stabilizes the orbital order. This orbital ordering pattern is also favored by superexchange interactions.[11] Since the orbital occupation determines the magnetic interaction via the Goodenough-Kanamori-Anderson rules, the antiferro-orbital order is directly connected to a special type of magnetic order. In this case the orbital ordering induces the so-called *A*-type antiferromagnetic order, where the spins are coupled ferromagnetically in the $ab$ planes while the $ab$ planes are coupled antiferromagnetically along the $c$ direction.[12] This example illustrates the intimate relation between magnetism, structure, and orbitals.

Upon doping with divalent ions, Jahn-Teller-active $Mn^{3+}$ sites are (formally) replaced by Jahn-Teller-inactive $Mn^{4+}$ sites. Furthermore, this introduces the charge degree of freedom leading to charge ordering phenomena at certain dopings. A prototype for the simultaneous ordering of charge, spin, and orbital degrees of freedom is the so-called CE phase which develops at half doping.[7,12–14] In this insulating phase ferromagnetic charge- and orbital-ordered zig zag chains develop along the *b* direction which are coupled antiferromagnetically along the *a* direction. Successive $ab$ planes are aligned antiferromagnetically along the *c* direction while the charge and orbital ordering pattern is the same. Indications for the development of a charge-, spin-, and orbital ordered-ground state are also found in the underdoped regime. In particular, there is evidence for the onset of charge order in the ferromagnetic insulating (FMI) phase of $La_{1-x}Sr_xMnO_3$ with $x \sim 1/8$ (Refs. 15 and 16). However, in this case the development of charge order is less established: While the superstructure reflections observed in the FMI phase by neutron and hard x-ray scattering[17–19] have been interpreted in terms of charge order, the results from a previous resonant x-ray scattering (RXS) study seem to disagree with this interpretation.[20] Instead, this RXS study indicates the presence of orbital ordering in the FMI phase. Furthermore, the microscopic structure of the FMI phase of $La_{7/8}Sr_{1/8}MnO_3$ is still the subject of intense discussions and several models for the charge and orbital ordering pattern have been suggested.[18,20–23]

In this paper we present a RXS study on $La_{7/8}Sr_{1/8}MnO_3$ single crystals. The symmetry-forbidden (300) reflection is observed when the energy of the incident photons is tuned to the Mn *K* edge and, moreover, its inte-

 

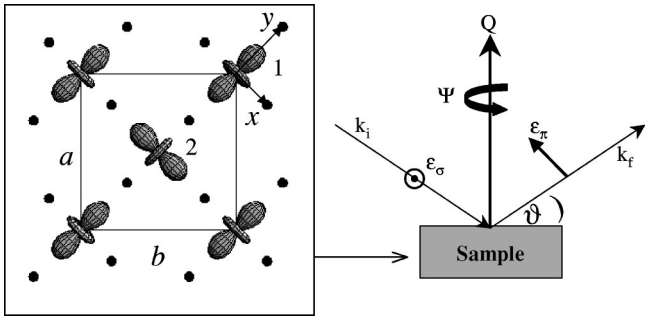


FIG. 1. *Left:* view of the $ab$ plane in the orbital-ordered state of $LaMnO_3$ (grey lobes, occupied $3d$ orbital; solid circles, oxygen). The crystal axes correspond to the orthorhombic *Pbnm* setting which is used throughout this paper. *Right:* sketch of a RXS experiment. At the (300) reflection in the orbital-ordered phase of $LaMnO_3$ the polarization of the incident beam ($k_i$, $\epsilon_\sigma$) is rotated into the scattering (paper) plane ($k_f$, $\epsilon_\pi$). During an azimuthal scan the sample is rotated around the scattering vector **Q**.

grated intensity is found scale with structural distortions. In particular, the integrated intensity of the (300) reflection is strongest between $T_{CO}=150\,\mathrm{K}$ and $T_{JT}=270\,\mathrm{K}$. The pronounced enhancement of the resonant intensity in this temperature regime, the rotation of the beam polarization from $\sigma$ to $\pi$ ($\sigma\pi$ scattering), the $\sin^2$-azimuthal dependence, and the temperature dependence of the lattice constants provide firm experimental evidence for the presence of an orbital-ordered state between $T_{CO}$ and $T_{JT}$ which is similar to that found in $LaMnO_3$. Upon cooling the integrated intensity of the (300) reflection collapses at the metal-insulator transition at $T_{CO}$ and the resonant (1.5 1.5 3) reflection emerges. At this position a resonance is observed in the $\sigma\pi$ as well as in the $\sigma\sigma$ channel (in addition to a nonresonant contribution in $\sigma\sigma$) and, moreover, the resonant intensities in both channels display an azimuthal dependence. The suppression of the (300) reflection and the occurrence of the (1.5 1.5 3) reflection signal a rearrangement in the orbital sector which is connected to the metal-insulator transition of $La_{7/8}Sr_{1/8}MnO_3$. Finally, we discuss the fact that the results presented in this paper seem to contradict the observations of a previous RXS study and show that this disagreement can be resolved by taking into account the twin structure of perovskites.

## II. EXPERIMENTAL TECHNIQUES

The RXS technique is well suited for the investigation of correlations between different degrees of freedom, because it provides the possibility to observe charge, spin, and orbital degrees of freedom in a single experiment. Moreover, the energy and azimuthal dependences of a given reflection give further information about underlying order parameters. In the following we will discuss the main features of an RXS experiment using $LaMnO_3$ as an example. As demonstrated in the left part of Fig. 1 the onset of the antiferro-orbital order results in two inequivalent Mn sites (sublattices 1 and 2 in Fig. 1) where the $e_g$ electron occupies a different orbital state. When the x-ray energy is tuned to the Mn $K$ edge the scattering process involves $1s\rightarrow 4p$ transitions—i.e., the creation of virtual photoelectrons in an intermediate $4p$ state. In the orbital-ordered phase the $4p$ states have different energies $E_\gamma(4p_j)=\hbar\omega_0+\Delta_j^\gamma$, where $j=x,y,z$ denotes the different $4p$ states pointing along the three principal axes of the $MnO_6$ octahedra and $\gamma=1,2$ refers to the sublattice.[9] Therefore, assuming atomic $4p$ states and using the dipole approximation the relevant term of the atomic form factor around the Mn $K$ edge can be written as $\Delta f=\boldsymbol{\epsilon}_f^t\cdot\hat{f}\cdot\boldsymbol{\epsilon}_i$, with the initial and final polarization vector $\boldsymbol{\epsilon}_{i,f}$ and the second rank tensor $\hat{f}$ defined by[24,25]

$$\hat{f}_\gamma^{(\alpha,\beta)}=\frac{1}{m}\sum_j\frac{\langle 1s|p_\beta|4p_j\rangle\langle 4p_j|p_\alpha|1s\rangle}{E_\gamma(4p_j)-E(1s)-\hbar\omega-i\Gamma/2}\qquad(1)$$

($p_\beta$: component of the momentum operator). This tensor has the symmetry of the Mn-site's local environment. More specifically, on sublattice 1 we have $\Delta_y^1=-2\Delta$ and $\Delta_x^1=\Delta_z^1=\Delta$ (see Ref. 9), leading to

$$\hat{f}_1=\begin{pmatrix} f_\parallel & 0 & 0\\ 0 & f_\perp & 0\\ 0 & 0 & f_\perp\end{pmatrix},$$

with the following energy-dependent matrix elements:

$$f_\perp=f_1^{yy}=\frac{A}{\hbar(\omega_0-\omega)-2\Delta-i\Gamma/2},$$

$$f_\parallel=f_1^{xx}=f_1^{zz}=\frac{A}{\hbar(\omega_0-\omega)+\Delta-i\Gamma/2}$$

($A$: positive constant $\times$ eV). Please note that no assumption has been made about the origin and sign of the splitting $\Delta$. This issue is still hotly debated[26–30] and we will come back to this point later.

In order to calculate the structure factor tensor $F_{300}=\hat{f}_1-\hat{f}_2$ in the orbital-ordered phase of $LaMnO_3$, it has to be taken into account that the roles of $x$ and $y$ are exchanged on the sublattices 1 and 2. After the transformation of $F$ into the orthorhombic crystal frame one gets

$$F_{300}=2\times\begin{pmatrix} 0 & f_\parallel-f_\perp & 0\\ f_\parallel-f_\perp & 0 & 0\\ 0 & 0 & 0\end{pmatrix}.$$

The tensorial character of $F_{300}$ expresses the fact that due to the anisotropic form factors the scattering process depends on the polarization of the incident and scattered beams.[31–33] The scattering amplitude can then be calculated as $A_{if}=\boldsymbol{\epsilon}_f^t\cdot F_{300}\cdot\boldsymbol{\epsilon}_i$. Using the polarization vectors for $\sigma$- and $\pi$-polarized light expressed in the crystal frame,

$$\boldsymbol{\epsilon}_\sigma=(0,\cos\psi,\sin\psi),$$

$$\boldsymbol{\epsilon}_\pi=(\cos\vartheta,\sin\vartheta\cos\psi,\sin\vartheta\sin\psi),$$

where $\psi$ is the azimuthal and $\vartheta$ is the Bragg angle (Fig. 1). It follows for the intensity in the $\sigma\pi$and the $\sigma\sigma$ channels

$$I_{\sigma\pi} \sim [(f_{\parallel} - f_{\perp}) \cos\vartheta \cos\psi]^2,$$

$$I_{\sigma\sigma} = 0.$$

Therefore, the calculation based on the energy splitting of the $4p$ states reproduces the experimental observations of an RXS experiment on $LaMnO_3$—namely the pure $\sigma\pi$ scattering, the $\sin^2$-azimuthal dependence, and the dipolar-type resonance at the Mn $K$ edge.[9]

In general, anisotropic atomic form factors can lead to the occurrence of glide plane- or screw-axis-forbidden reflections.[31,34] Since the anisotropy of $f$ is connected to the anisotropy of the x-ray susceptibility, reflections of this type are called Anisotropy of the Tensor of Susceptibility (ATS) reflections. The (300) reflection in $LaMnO_3$ is an example for such an ATS reflection, because it is glide-plane forbidden in *Pbnm* symmetry and occurs due to the anisotropy of the atomic form factors.

The RXS experiment on $La_{7/8}Sr_{1/8}MnO_3$ presented in this paper has been performed using a vertical scattering geometry at the wiggler beamline W1 at HASYLAB. This beamline is equipped with a Si(111) double monochromator which provides an energy resolution at the Mn $K$ edge of about 2 eV. The sample was mounted on the cold finger of a closed-cycle cryostat which was itself mounted on a standard Eulerian cradle. The incident slits have been chosen in order to give a polarization $P = I^{\sigma}/(I^{\sigma} + I^{\pi}) = 0.95$ of the incident beam. For the polarization analysis at the Mn $K$ edge the copper (220) reflection with a scattering angle of $2\Theta \simeq 95.48°$ has been used, leading to a cross talk between $\sigma\sigma$ and $\sigma\pi$ channels of 3% as determined at the (400) position. The $La_{7/8}Sr_{1/8}MnO_3$ single crystals have been grown using the traveling floating zone method[35] and for the RXS experiment samples with a polished (100) and (112) surfaces have been prepared. For the macroscopic characterization magnetization measurements using a vibrating sample magnetometer have been performed.[36] Furthermore, the thermal expansion has been measured utilizing a capacitance dilatometer which allows a very accurate study of crystal length changes.[37] The resistivity measurements have been done using the standard four-probe technique.

## III. RESULTS

### A. Macroscopic Measurements

Figure 2 deals with a comparison between the temperature dependences of the macroscopic sample length $dL/L$, the magnetization $M$, and the electrical resistivity $\rho$. The three successive phase transitions at $T_{JT} \simeq 270$ K, $T_C \simeq 183$ K, and $T_{CO} \simeq 150$ K are clearly observable in all three quantities: Upon cooling, the structural phase transition into the cooperative Jahn-Teller distorted phase[38] at $T_{JT}$ is signaled by a jumplike increase of $dL/L$. At $T_{JT}$ the magnetic interactions and the electronic structure also change as revealed by the anomalies of $M$ and $\rho$. Cooling the sample down to $T_C$, the onset of ferromagnetic order is signaled by the increase of $M$.

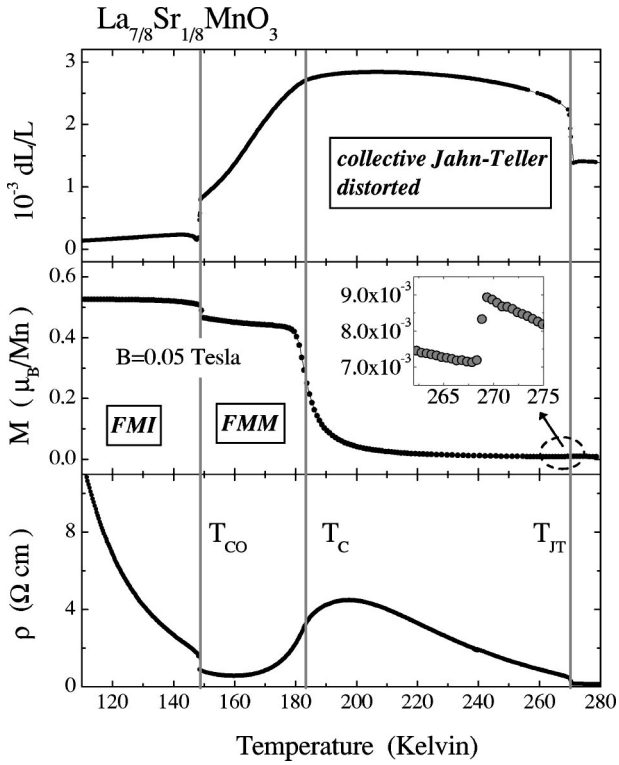


FIG. 2. Comparison between the temperature dependences of the macroscopic sample length $dL/L$ (*top*), the magnetization (*middle*), and the electrical resistivity (*bottom*).

The ferromagnetic spin alignment is connected to a metallic characteristics of $\rho$ in agreement with the double-exchange picture. Therefore, this phase is called ferromagnetic metallic (FMM), although the resistivity is still three orders of magnitude larger than that of a typical metal. The enhanced charge carrier mobility with decreasing temperature correlates with a continuous reduction of the cooperative Jahn-Teller distortions as indicated by the reduction of $dL/L$ below $T_C$. At $T_{CO}$ the cooperative Jahn-Teller distortions are strongly suppressed as signaled by the jumplike decrease of $dL/L$ upon cooling. Moreover, at this phase transition both the magnetization *and* the resistivity display an abrupt increase in contradiction to a bare double-exchange picture. Furthermore, the characteristics of the electrical resistivity change from metallic to insulating. In what follows we will refer to this ferromagnetic insulating phase as the FMI phase.

### B. Twin domains

In our RXS study two differently oriented samples have been investigated: one sample with a (100) surface and another sample with a (112) surface. Hereafter, we will refer to these samples as $S1$ and $S2$, respectively. Due to the twinning, the (100)-oriented sample contains (010)-oriented twin domains and it can also contain (112)-oriented twin domains and vice versa. As a result the (400), (040), and (224) reflections can, in principle, emerge at the same position. However, the different temperature dependences of the corresponding lattice plane spacings allow us to exclude the superposition of the (224) and (400)/(040) reflections in our

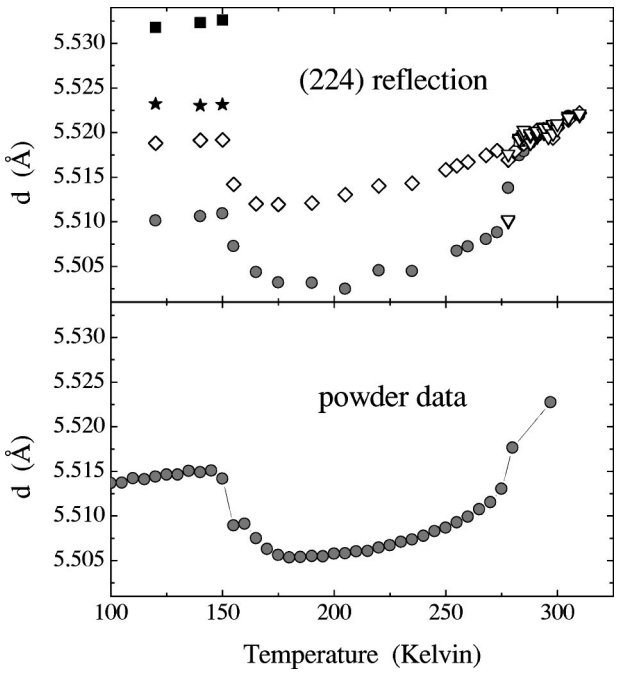


FIG. 3. Comparison between the temperature dependences of the lattice plane spacings derived from the scattering angles of all reflections found around the (400) position of *S*2 (*top*) and the temperature dependence of the (224) lattice plane spacing calculated from the lattice parameters (*bottom*).

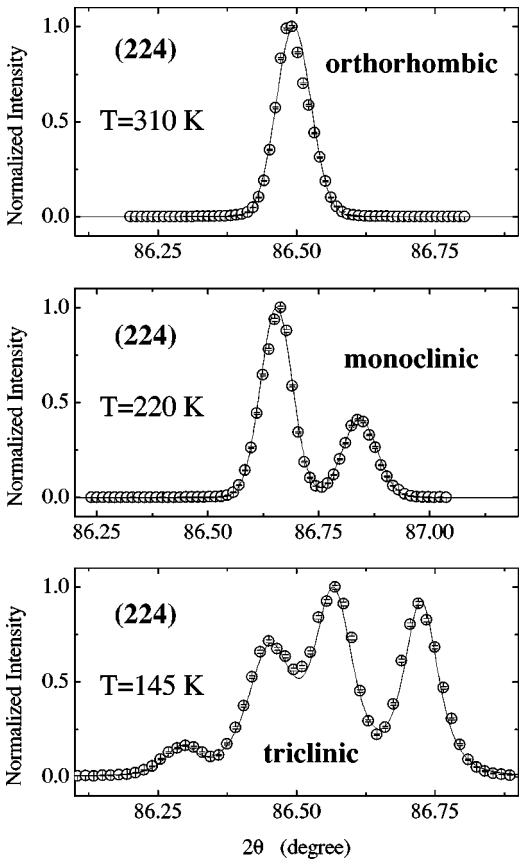


FIG. 4. Radial scans at through the (224) reflection at different temperatures. The lines are fitted Gaussian functions serving as guides to the eye.

samples. To be more specific, from the temperature dependence of the lattice parameters[39] it follows that the (400) and (040) lattice plane spacings both increase at the phase transitions into the cooperative Jahn-Teller distorted phase, whereas the (224) lattice plane spacing decreases. In this manner, the two reflections observed for *S*1 at slightly different scattering angles around the nominal (400) position have been identified as (400) and (040) reflections (compare Fig. 6); i.e., only twins with interchanged *a* and *b* axis have been found for sample *S*1. In the upper part of Fig. 3 the temperature dependences of the lattice plane spacings derived from the scattering angles of all reflections observed around the nominal (224) position of *S*2 are given. From these temperature dependences we can rule out the presence of (400) and (040) reflections at this position, because upon cooling none of the observed lattice plane spacings increases at $T_{JT}$ or decreases at $T_{CO}$. The lower part of Fig. 3 shows the (224) lattice plane spacing which has been calculated using lattice parameters obtained by powder diffraction and assuming an orthorhombic symmetry. The reduction of the lattice plane spacing in the cooperative Jahn-Teller distorted phase is evident. However, for a comparison between the data shown in the lower and upper parts of Fig. 3 it has to be taken into account that the symmetry below $T_{JT}$ is no longer orthorhombic. As a result of the reduction of the lattice symmetry from orthorhombic to monoclinic at $T_{JT}$ upon cooling two different lattice plane spacings are observed at the (224) position.[40] Below $T_{CO}$ the crystal symmetry is reduced further to triclinic[40] leading to the occurrence of four different scattering angles corresponding to the (224), $(2\bar{2}4)$, $(22\bar{4})$ and $(2\bar{2}\bar{4})$ reflections. The reduction of the crystal symmetry upon lowering the temperature is further illustrated in Fig. 4 where radial $(\Theta/2\Theta)$ scans at the (224) position are displayed. The single peak observed at 310 K$>T_{JT}$ splits in the cooperative Jahn-Teller distorted phase (e.g., at 220 K) into two reflections. The triclinic symmetry below $T_{CO}$ is signaled by a fourfold splitting of the (224) reflection at 145 K$<T_{CO}$. Therefore, these observations are in perfect agreement with results from high-resolution powder diffraction measurements and it can be concluded that the surface prepared on *S*2 is a (112) surface.

The absence of (112)-oriented twin domains in *S*1 and the absence of the (100)-oriented twin domains in *S*2 are both the result of a special twin structure. This twin structure is most likely the consequence of the parameters which have been used for growing the batch in the floating zone furnace.

### C. The (300) reflection

In this section we discuss the results of the RXS measurements on sample *S*1. In Fig. 5 a fluorescence measurement at room temperature, the energy dependence of the symmetry-forbidden (300) reflection at 200 K in the $\sigma\pi$ channel, and the azimuthal dependence of the resonant intensity at 200 K are shown. The comparison between the fluorescence measurement given in Fig. 5(a) and the energy

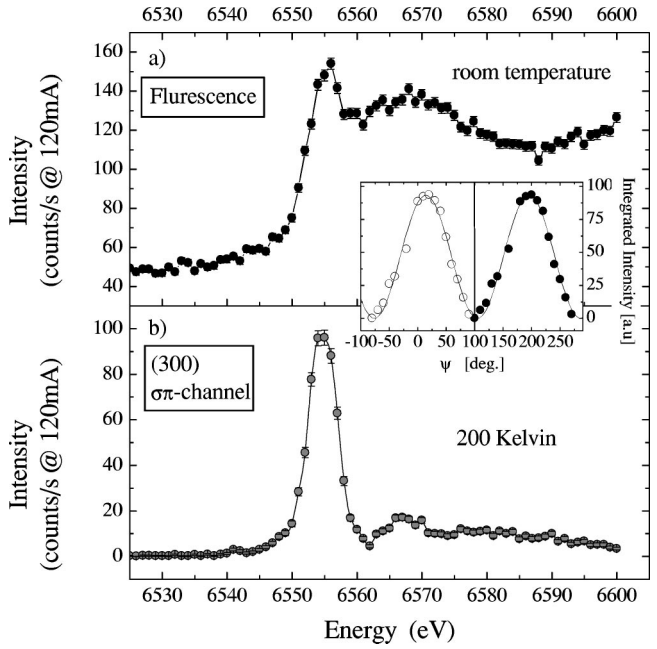


FIG. 5. (a) Fluorescence measurement taken at room temperature. (b) Energy dependence of the (300) reflection at 200 K. The azimuthal dependence of the (300) reflection also taken at 200 K is given in the inset.

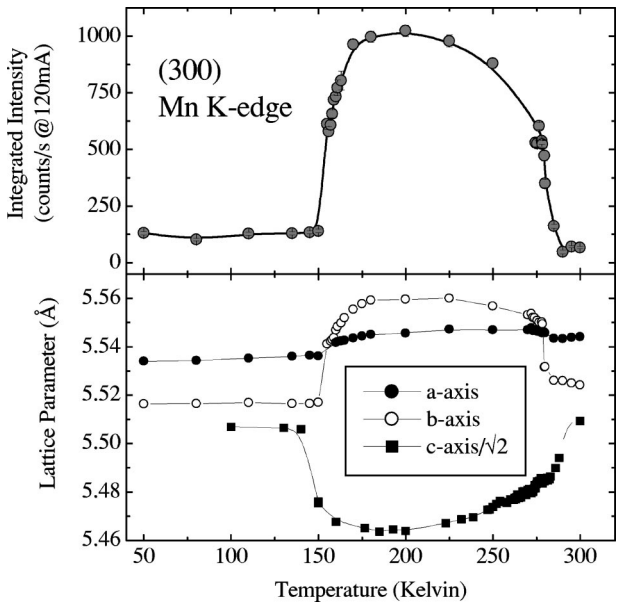


FIG. 6. *Top:* temperature dependence of the integrated intensity of the (300) reflection at 6555 eV for $\psi=0°$. The integrated intensity has been calculated by integrating over radial, rocking, and $\chi$ scans. *Bottom:* temperature dependence of the lattice parameters (*Pbnm* setting). The *a* and *b* parameters have been obtained from the reflections observed around the (400) position of sample *S*1. The *c*-parameter has been measured using a (001)-oriented sample.

dependence displayed in Fig. 5(b) shows around the Mn *K* edge a strong increase of the intensity at the (300) position. Its maximum is slightly above the Mn *K* edge, which proves the dipolar character of the involved virtual transition. Furthermore, the intensity of the (300) reflection displays a pronounced azimuthal dependence as demonstrated in the inset of Fig. 5. The $\sin^2\psi$ behavior of the resonant intensity is clearly observed. Note that the data points represented by closed circles have been obtained from the measured data (open symbols) by a translation along the $\psi$ axis about 180°. The polarization analysis which has been carried out using the (220) reflection of a copper analyzer crystal shows that within the experimental resolution the resonant scattering at the (300) position occurs only in the $\sigma\pi$ channel. The above fingerprints of the resonant signal at 200 K—namely, the $\sigma\pi$-scattering and $\sin^2$-azimuthal dependences—agree with the results of a RXS study on $LaMnO_3$ in the orbital-ordered phase.[9] Moreover, the above observations are reproduced by the calculation presented in Sec. II which was based on the energy splitting of atomic $4p$ states and the orbital ordering pattern shown in Fig. 1. Therefore, the RXS results on $La_{7/8}Sr_{1/8}MnO_3$ at 200 K reveal the presence of an orbital-ordered and cooperative Jahn-Teller distorted phase at 200 K which is similar to that of $LaMnO_3$.

Figure 6 deals with a comparison between the integrated intensity of the (300) reflection and the lattice parameters. It is evident that the integrated intensity $I_{300}$ strongly increases in the cooperative Jahn-Teller-distorted phase between $T_{CO}$ and $T_{JT}$ which is signaled by a pronounced elongation of the $a,b$ parameters and a contraction of the $c$ parameter at $T_{JT}$. The anomalies observed in the lattice parameters are in agreement with the orbital ordering pattern displayed in Fig. 1: The antiferro-orbital order of Jahn-Teller-distorted $MnO_6$-octahedra inside the $ab$ plane results in a shortening of the Mn-O bond length along the $c$ direction and a reduction of the corresponding lattice parameter. The observed anomaly in the $a,b$, parameters is a consequence of the antiferro-orbital ordering in the presence of octahedral tilts.[41] With further decreasing temperature $I_{300}$ and the structural distortions reflected by the lattice parameters increase, reaching a maximum at $T_C$. With the onset of ferromagnetic order and enhanced charge carrier mobility below $T_C$ the cooperative Jahn-Teller distortions are gradually reduced and disappear abruptly at $T_{CO}$. Finally we mention that the temperature, energy, and polarization dependences of the (300) and the (030) peak are the same within the errors of the experiment.

From the temperature dependences shown in Fig. 6 it is clear that $I_{300}$ is directly connected to lattice distortions. This is further illustrated in Fig. 7 where a comparison between the structural parameter $\xi=a/(c/\sqrt{2})$ and $I_{300}$ is shown. Obviously, $I_{300}$ scales as $\xi$ in the investigated temperature range. It can be concluded that both quantities measure the same order phenomenon—namely, the antiferrodistortive order of Jahn-Teller-distorted $MnO_6$ octahedra between $T_{CO}$ and $T_{JT}$, which is connected to an orbital ordering pattern similar to that shown in Fig. 1. Note, that the (300) reflection does not vanish completely below $T_{CO}$ and above $T_{JT}$. The above results seem to contradict contradict the findings of a previous RXS study.[20] In this study, the (300) reflection has been observed only in the FMI phase below $T_{CO}$. On the contrary, we observe the (300) reflection in the whole temperature

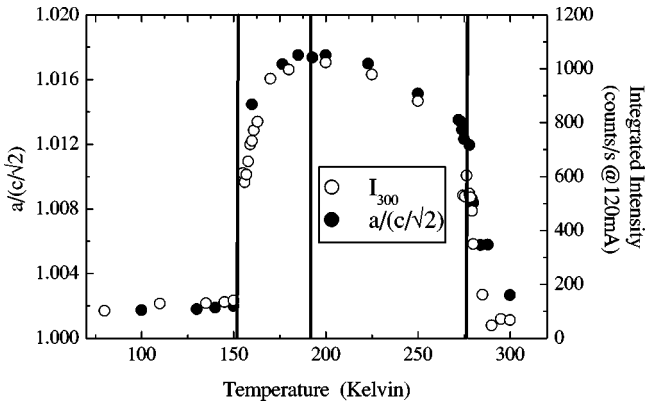


FIG. 7. Temperature dependence of $\xi = a/(c/\sqrt{2})$ (solid symbols) and $I_{300}$ (open symbols).

range under investigation. This discrepancy can be resolved by taking into account the twinning of the samples as will be discussed now.

### D. (1.5 1.5 3) reflection

As already mentioned above, due to the twinning of the samples, the (400) and (224) reflections of different twin domains can occur around the same position. As a consequence, the (300) position of one twin domain corresponds to the (1.5 1.5 3) position of another domain. In order to study the resonant scattering at the (1.5 1.5 3) position, the (112)-oriented sample *S*2 has been investigated. As demonstrated in Fig. 8 the suppression of the $I_{300}$ reflection coincides with the occurrence of the (1.5 1.5 3) reflection in $\sigma\pi$ as well as in the $\sigma\sigma$ channel below $T_{CO}$. The observation of this reflection is in agreement with results from a recent electron diffraction study.[42] It can be seen that the integrated intensity in the $\sigma\pi$ as well as in the $\sigma\sigma$ channel slightly decreases again upon cooling down to 50 K. Furthermore, we observe a strong suppression of the resonant intensity below 50 K due to the irradiation effect[43] (cf. Fig. 11).

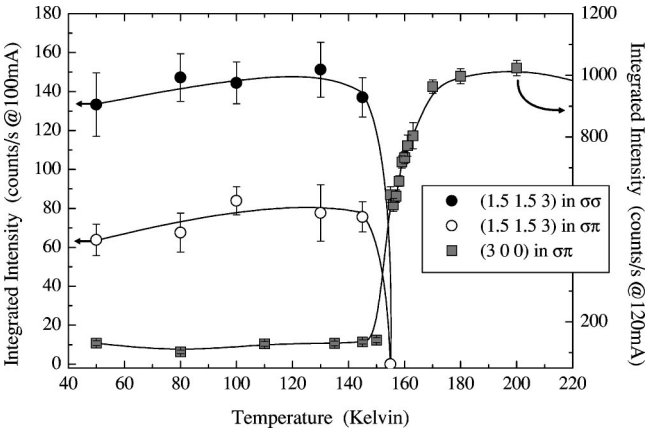


FIG. 8. Temperature dependence of the integrated intensity of the (1.5 1.5 3) reflection in the $\sigma\sigma$ and the $\sigma\pi$-channels (open and solid circles). The integrated intensity of the (300) reflection is also shown (gray squares). The intensities have been obtained by integrating over radial, rocking, and $\chi$ scans.

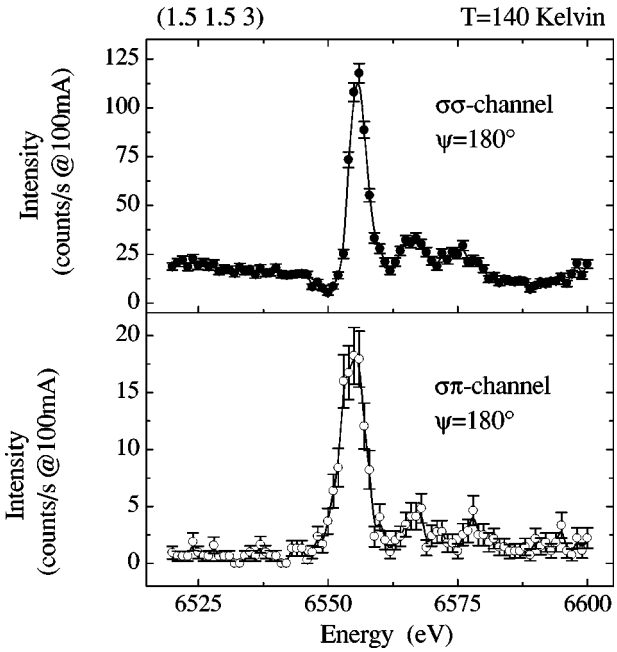


FIG. 9. Energy dependence of the (1.5 1.5 3) reflection in the $\sigma\sigma$ and $\sigma\pi$ channels at 140 K. The polarization analysis has been performed using the (220) reflection of copper.

Note, that the observed temperature dependence further strengthens our conclusion that the (112) surface of sample *S*2 does not contain (100) surfaces of differently oriented twin domains (compare Fig. 6). The polarization analysis of the measurement shown in Fig. 8 has been performed using the (002) reflection of graphite corresponding to a scattering angle $2\Theta = 68.4°$ at the Mn *K* edge. Since $2\Theta$ is considerably smaller than 90°, there are significant contributions of the $\sigma\sigma$ scattering in the $\sigma\pi$ channel and vice versa (cross talk $\simeq 15\%$). However, the signal observed in the $\sigma\pi$ channel is considerably larger than the signal due to the cross talk which is about $\simeq 20$ counts/s. A simple calculation taking into account the incomplete $\sigma$ polarization of the incident beam and the cross talk effects yields $I_{\sigma\sigma}/I_{\sigma\pi} \simeq 2.25$. In order to reduce the cross talk, the following measurements have been performed using the (220) reflection of copper ($2\Theta = 95.46°$ at 6554 eV, cross talk: 3 %). The energy dependence of the (1.5 1.5 3) reflection is given in Fig. 9. Note that the intensity maximum at a particular position in reciprocal space is shown in Fig. 9 which differs from the integrated intensities given in Fig. 8.

In both channels a main resonance at 6554 eV and the typical structure at higher energies is observed. However, while the intensity in the $\sigma\pi$ channel vanishes far above and below the Mn *K* edge, the signal in the $\sigma\sigma$ channel also contains a nonresonant contribution. The nonresonant scattering at the (1.5 1.5 3) position reveals a long-ranged superstructure modulation occurring in FMI-phase. Note, that this implies that the (1.5 1.5 3) reflection is no ATS reflection. Nevertheless, the resonant signal at the (1.5 1.5 3) position shows that this superstructure modulation is connected to anisotropies of the manganese form factors.

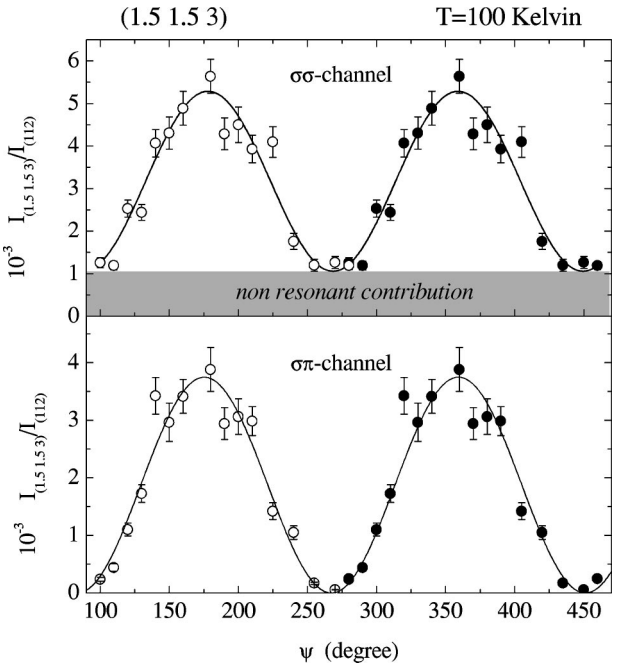


FIG. 10. Azimuthal dependence of the integrated intensity measured at the (1.5 1.5 3) position at 100 K. The open symbols represent the measured data while the solid symbols have been obtained by translating the measured data by 180°. The solid line is a fit to a $\sin^2$ behavior.

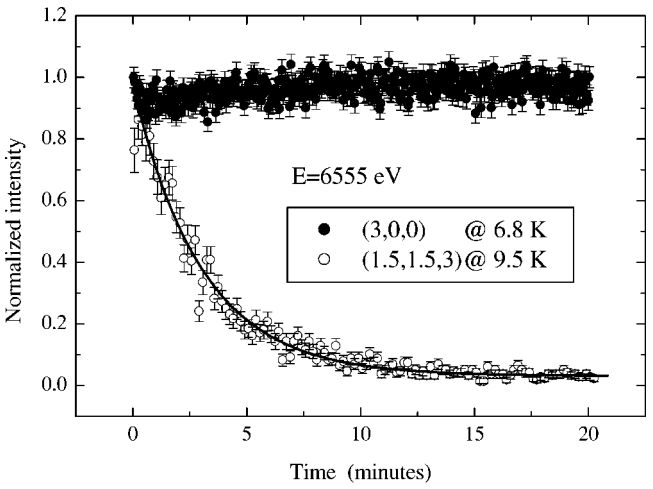


FIG. 11. Comparison between the irradiation effect observed at the (1.5 1.5 3) and the (300) position. A fit to an exponential decay is indicated by the solid line. The measurement at the (300) position has been performed without an analyzer. For the data taken at the (1.5 1.5 3) position a copper analyzer has been used.

Besides the resonant behavior the intensity of the (1.5 1.5 3) reflection also displays a pronounced azimuthal dependence as shown in Fig. 10. In particular, the integrated intensity reaches a maximum around $\psi = 180°$—i.e., when the incident polarization lies parallel to the $(11\bar{2})$ direction. Upon increasing $\psi$ from 180° to 270° the intensity of the (1.5 1.5 3) reflection in both channels is continuously reduced to its minimum. At this azimuthal angle the polarization is parallel to the $(1\bar{1}0)$ direction. Note that the reflection observed in the $\sigma\sigma$ channel does not vanish completely at $\psi = 270°$ due to the nonresonant signal, while the intensity in the $\sigma\pi$ channel is reduced to the background level. Interestingly, within the experimental errors the azimuthal dependence observed in both channels is the same, indicating a common origin for both signals. To summarize, the azimuthal dependence and the rotation of the beam polarization again reveal the presence of an anisotropic form factor. Moreover, the resonance at the Mn *K* edge shows that this anisotropy is connected to the $4p$ intermediate states (compare Sec. II). Finally, the nonresonant contribution at the (1.5 1.5 3) position reveals a long-ranged structural modulation which occurs at the metal-insulator transition. All these observations can be naturally understood in terms of orbital order, since this order parameter couples to the splitting of the $4p$ states and to the structure.

Concerning the splitting of the $4p$ states it has to be noted that there are several mechanisms which can produce such an energy splitting. The on-site Coulomb interaction between the occupied $e_g$ state and the $4p$ states is one candidate.[26] Another intensively discussed mechanism is the reduction of the hybridization between the oxygen $2p$ states and the manganese $4p$ states due to a distortion of the $MnO_6$ octahedra.[27,29] However, also in this case the splitting of the $4p$ states is connected to the orbital degree of freedom, because a distortion of a $MnO_6$ octahedron lifts the degeneracy of the $e_g$ states and determines the orbital occupation at a given site.

We conclude that the above RXS results evidence a rearrangement of the orbital ordered state at $T_{CO}$. Moreover, the observed energy, azimuthal, and temperature dependences of the (1.5 1.5 3) reflection resemble the RXS results at the (030) position published in Ref. 20. We argue that the reflection observed in Ref. 20 at the nominal (030) position corresponds to the (1.5 1.5 3) reflection investigated in the present study.

### E. Irradiation effect at low temperatures

Upon irradiation at low temperatures the FMI phase of $La_{7/8}Sr_{1/8}MnO_3$ decays into another insulting phase.[43,44] This irradiation effect has also been observed in the present study, as demonstrated in Fig. 11. Focusing on the (1.5 1.5 3) reflection, a rapid decay of the maximum intensity is observed when the sample is irradiated with 6555-eV photons at 9.5 K. The solid line in Fig. 11 is a fit to an exponential decay of the form $I(t) = B + I_0\, e^{-t/\tau}$ with $\tau \simeq 3$ min. After 30 min no detectable intensity at the (1.5 1.5 3) position is observed in the $\sigma\pi$ as well as in the $\sigma\pi$ channel; i.e., the (1.5 1.5 3) reflection vanishes completely upon irradiation. Contrary to the pronounced effect found at the (1.5 1.5 3) position, the (300) reflection stays almost constant across the radiation-induced phase transition.

As the irradiation with x rays around the Mn *K* edge has a strong impact on the electronic states of manganese, the decay of the (1.5 1.5 3) reflection further supports the conclusion that the corresponding superstructure modulation is tightly coupled to the electronic degrees of freedom. In fact, we do not observe the irradiation effect when the sample is

irradiated with 100 keV x rays at low temperatures; i.e., the effect does not occur far away from any absorption edge. The time dependence of the (300) reflection, on the other hand, reveals that the anisotropies which lead to the occurrence of the (300) reflection below $T_{CO}$ are not connected to the electronic states of manganese.

### F. Discussion of the RXS results

It is important to stress once again that the coupling mechanism between the orbital degree of freedom and the RXS signal is still the subject of intense discussions. However, the nonvanishing intensity of the (300) reflection above $T_{JT}$—i.e., in the phase without static orbital order—strongly indicates that anisotropic form factors are not only determined by the occupied $e_g$ states alone. For example, a steric distortion of the $MnO_6$ octahedra can induce an anisotropic form factor which leads to the occurrence of ATS-reflections and, in particular, to the non-vanishing (300) reflection. Take note that below $T_{CO}$ the symmetry of the lattice is triclinic $(P\bar{1})$ so that the (300) reflection is allowed. However, the resonant behavior of this reflection indicates that the corresponding selection rule is at least approximately conserved in the triclinic phase.

According to the observations made at the (300) position one may argue that the resonant scattering at the (1.5 1.5 3) position is not necessarily connected to orbital order, either. However, in the case of the (1.5 1.5 3) reflection the situation is different. First of all, this superlattice reflection is only observed in the FMI phase and, more importantly, the scattering contains resonant as well as nonresonant contributions. The nonresonant scattering at the (1.5 1.5 3) position signals a superstructure modulation which develops at the metal-insulator transition. The onset of the structural modulations with a concomitant change of the electronic structure constitutes a strong indication for the coupling between the structural modulations and the electronic degrees of freedom. This conclusion is further supported by the irradiation effect described above. Concerning the resonant scattering at the (1.5,1.5,3) position, the observed temperature dependence as well as the irradiation effect indicates that also this contribution is related to the manganese $e_g$ states.

Although the temperature dependence of the (300) reflection indicates that RXS at the Mn $K$ edge only indirectly probes the orbital degrees of freedom, the experimental observations as a whole provide firm experimental evidence that the scattering at (1.5,1.5,3) position signals a long-range ordering of electronic states on the manganese sublattice—i.e., orbital and/or charge order. We conclude that the metal-insulator transition of $La_{7/8}Sr_{1/8}MnO_3$ is accompanied by an orbital rearrangement which involves a transformation of the antiferro-orbital ordering above $T_{CO}$ into another type of orbital order below $T_{CO}$.

One may speculate about the type of orbital order which occurs below $T_{CO}$ and gives rise to the ferromagnetic and insulating behavior. A possible scenario refers to the formation of orbital polarons at the metal insulator transition.[23,45] Since orbital polarons are ferromagnetic objects which lead to a pronounced suppression of the charge carrier bandwidth, this scenario naturally explains the coexistence of ferromagnetic and insulating properties. In addition to this, macroscopic measurements on $La_{1-x}Sr_xMnO_3$ with $x \sim 1/8$ revealed the important role of the magnetic degrees of freedom for the metal-insulator transition.[15] This observation is also in agreement with the formation of orbital polarons, because these objects are stabilized by the double-exchange interaction. Although it is difficult to guess the microscopic arrangement of the orbital polarons in the FMI phase based on the RXS data presented above, we mention that the observed superstructures are consistent with the orbital polaron lattice obtained by Hartree-Fock calculations.[23] Based on these experimental and theoretical results, we speculate that an orbital polaron lattice develops in $La_{7/8}Sr_{1/8}MnO_3$ below $T_{CO}$.

## IV. CONCLUSION

We have presented resonant x-ray scattering studies of $La_{7/8}Sr_{1/8}MnO_3$. At the Mn $K$ edge the resonant (300) reflection has been observed in the $\sigma\pi$ channel. In contrast to previously published results we observe a strong increase of the resonant intensity in the cooperative Jahn-Teller-distorted phase at temperatures between 150 K and 270 K. Below 150 K and above 270 K the intensity at the (300) reflection is reduced by a factor of 10. The occurrence of the resonant (300)-reflection at the Mn $K$ edge, the rotation of the beam polarization from $\sigma$ to $\pi$, the $\sin^2$-azimuthal dependence and the anomalies displayed by the lattice constants give strong experimental evidence for an orbital-ordered state similar to that of $LaMnO_3$. Furthermore, it follows that the temperature dependence, of the resonant (300) reflection does not allow one to draw any conclusions about the origin of the splitting of the $4p$ bands as suggested in Ref. 26.

Upon cooling the $I_{300}$ collapses at $T_{CO}$ and the resonant (1.5 1.5 3) reflection emerges. At this position a resonant signal is observed in the $\sigma\pi$ and $\sigma\sigma$ channels. Moreover, a nonresonant contribution in the $\sigma\sigma$ channel shows that the underlying order phenomenon is connected to static structural modulations. The resonant signal in both channels has been found to display the same azimuthal and temperature dependences indicating that the resonant signal in the $\sigma\sigma$ and $\sigma\pi$ channels has a common origin. We note that the disagreement between a previous and the present RXS study can be understood by taking into account the twinning of $La_{1-x}Sr_xMnO_3$. In particular, we argue that the (300) reflection in Ref. 20 corresponds to a (1.5 1.5 3) reflection for the following reasons: First, the azimuthal and energy dependences of the (1.5 1.5 3) reflection agree with the results published in Ref. 20, although a polarization analysis has not been performed in Ref. 20. Second, the temperature dependences are also similar. The pronounced decrease of the resonant intensity reported in Ref. 20 can be understood in terms of the low-temperature instability of the FMI phase—i.e., the irradiation effect. In particular, the (1.5 1.5 3) reflection observed in the present study vanishes under irradiation at low temperatures, corresponding to the pronounced decrease of the resonant intensity below 50 K observed in Ref. 20.

The results from the RXS studies on sample $S1$ and $S2$

thus indicate that the wave vector corresponding to the orbital ordering changes at $T_{CO}$, revealing an orbital rearrangement. Though a determination of the orbital ordering wave vector for the FMI phase is not possible from the above results, the RXS data presented in this article provides firm experimental evidence for the crucial role of the orbital degree of freedom at the metal-insulator transition of $La_{1-x}Sr_xMnO_3$ with $x \sim 1/8$.

**ACKNOWLEDGMENTS**

We are very grateful to H. Dosch for his support. Furthermore, the authors would like to thank S. Uhlenbruck for providing the electrical resistivity data. We also thank M. v. Zimmermann for helpful discussions and a careful reading of our manuscript. This work is supported by the Deutsche Forschungsgemeinschaft.

[1] J.G. Bednorz and K.A. Müller, Z. Phys. B **64**, 189 (1986).
[2] J.M. Tranquada, J.E. Lorenzo, D.J. Buttrey, and V. Sachan, Phys. Rev. B **52**, 3581 (1995).
[3] J.M. Tranquada, B.J. Sternlieb, J.D. Axe, Y. Nakamura, and S. Uchida, Nature (London) **375**, 561 (1995).
[4] B. Büchner, M. Breuer, A. Freimuth, and A.P. Kampf, Phys. Rev. Lett. **73**, 1841 (1994).
[5] P. Radaelli, D.E. Cox, M. Marezio, and S.-W. Choeng, Phys. Rev. B **55**, 3015 (1997).
[6] R.M. Kusters, J. Singelton, D.E. Keen, R. McGreevy, and W. Hayes, Physica B **155**, 362 (1989).
[7] Y. Tokura and N. Nagaosa, Science **288**, 462 (2000).
[8] J. Rodriguez-Carvajal, M. Hennion, F. Moussa, A.H. Moudden, L. Pinsard, and A. Revcolevschi, Phys. Rev. B **57**, R3189 (1998).
[9] Y. Murakami, J.P. Hill, D. Gibbs, M. Blume, I. Koyama, M. Tanaka, H. Kawata, T. Arima, Y. Tokura, K. Hirota, and Y. Endoh, Phys. Rev. Lett. **81**, 582 (1998).
[10] M. Zimmermann *et al.*, Phys. Rev. B **64**, 064411 (2001).
[11] L.F. Feiner and A.M. Oleś, Phys. Rev. B **59**, 3295 (1999).
[12] E.O. Wollan and W.C. Koehler, Phys. Rev. **100**, 545 (1955).
[13] J. van den Brink, G. Khaliullin, and D. Khomskii, Phys. Rev. Lett. **83**, 5118 (1999).
[14] J. Geck, D. Bruns, C. Hess, R. Klingeler, P. Reutler, M.v. Zimmermann, S.-W. Cheong, and B. Büchner, Phys. Rev. B **66**, 184407 (2002).
[15] R. Klingeler, J. Geck, R. Gross, L. Pinsard-Gaudart, A. Revcolevschi, S. Uhlenbruck, and B. Büchner, Phys. Rev. B **65**, 174404 (2001).
[16] S. Uhlenbruck, R. Teipen, R. Klingeler, B. Büchner, O. Friedt, M. Hücker, H. Kierspel, T. Niemöller, L. Pinsard, A. Revcolevschi, and R. Gross, Phys. Rev. Lett. **82**, 185 (1999).
[17] Y. Yamada, O. Hino, S. Nohdo, R. Kanao, T. Inami, and S. Katano, Phys. Rev. Lett. **77**, 904 (1996).
[18] Y. Yamada, J. Suzuki, K. Oikawa, S. Katano, and J.A. Fernandez-Baca, Phys. Rev. B **62**, 11 600 (2000).
[19] T. Niemoeller, M.v. Zimmermann, S. Uhlenbruck, O. Friedt, B. Büchner, T. Frello, N. Andersen, P. Berthet, L. Pinsard, A.D. Léon-Guevara, A. Revcolevschi, and J.R. Schneider, Eur. Phys. J. B **8**, 5 (1999).
[20] Y. Endoh, K. Hirota, S. Ishihara, S. Okamoto, Y. Murakami, A. Nishizawa, T. Fukuda, H. Kimura, H. Nojiri, K. Kaneko, and S. Maekawa, Phys. Rev. Lett. **82**, 4328 (1999).
[21] M. Korotin, T. Fujiwara, and V. Anisimov, Phys. Rev. B **62**, 5696 (2000).
[22] T. Inami, N. Ikeda, Y. Murakami, I. Koyama, Y. Wakabayashi, and Y. Yamada, Jpn. J. Appl. Phys., Suppl. **38-1**, 212 (1999).
[23] T. Mizokawa, D.I. Khomskii, and G.A. Sawatzky, Phys. Rev. B **61**, R3776 (2000).
[24] S. Ishihara and S. Maekawa, Phys. Rev. B **62**, 5690 (2000).
[25] M. Takahashi, J. Igarashi, and P. Fulde, J. Phys. Soc. Jpn. **68**, 2530 (1999).
[26] S. Ishihara and S. Maekawa, Phys. Rev. Lett. **80**, 3799 (1998).
[27] I.S. Elfimov, V.I. Anisimov, and G.A. Sawatzky, Phys. Rev. Lett. **82**, 4264 (1999).
[28] M. Benfatto, Y. Joly, and C.R. Natoli, Phys. Rev. Lett. **83**, 636 (1999).
[29] P. Benedetti, J. van den Brink, E. Pavarini, A. Vigliante, and P. Wochner, Phys. Rev. B **63**, 060408(R) (2001).
[30] S. Ishihara and S. Maekawa, Rep. Prog. Phys. **65**, 561 (2002).
[31] V.E. Dmitrienko, Acta Crystallogr., Sect. A: Found. Crystallogr. **39**, 29 (1983).
[32] A. Kirfel and A. Petcov, Acta Crystallogr., Sect. A: Found. Crystallogr. **47**, 180 (1991).
[33] D.H. Templeton, Acta Crystallogr., Sect. A: Found. Crystallogr. **54**, 158 (1998).
[34] A. Kirfel and W. Morgenroth, Acta Crystallogr., Sect. A: Found. Crystallogr. **49**, 35 (1993).
[35] P. Reutler, O. Friedt, B. Büchner, M. Braden, and A. Revcolevschi, J. Cryst. Growth **249**, 222 (2003).
[36] S. Foner, Rev. Sci. Instrum. **27**, 548 (1956).
[37] T. Lorenz, U. Ammerahl, T. Auweiler, B. Büchner, A. Revcolevschi, and G. Dhalenne, Phys. Rev. B **55**, 5914 (1997).
[38] H. Kawano, R. Kajimoto, M. Kubota, and H. Yoshizawa, Phys. Rev. B **53**, R14 709 (1996).
[39] L. Pinsard, J. Rodriguez-Cavajal, and A. Revcolevschi, J. Alloys Compd. **262-263**, 152 (1997).
[40] D.E. Cox, T. Iglesias, E. Moshopoulou, K. Hirota, K. Takahashi, and Y. Endoh, Phys. Rev. B **64**, 024431 (2001).
[41] T. Proffen, R. DiFrancesco, S.J.L. Billinge, E.L. Brosha, and G.H. Kwei, Phys. Rev. B **60**, 9973 (1999).
[42] K. Tsuda, M. Tanaga, K. Hirota, and Y. Endoh, J. Phys. Soc. Jpn. **70**, 1010 (2001).
[43] V. Kiryukhin, Y.J. Wang, F.C. Chou, M.A. Kastner, and R.J. Birgeneau, Phys. Rev. B **59**, R6581 (1999).
[44] D. Casa, B. Keimer, M.v. Zimmermann, J.P. Hill, H.U. Habermeier, and F.S. Razavi, Phys. Rev. B **64**, 100404(R) (2001).
[45] R. Kilian and G. Khaliullin, Phys. Rev. B **58**, R11 841 (1998).